JOURNAL OF PROPULSION AND POWER
Vol. 25, No. 1, January–February 2009

Pressure Measurements and Attenuation in a Hybrid Multitube Pulse Detonation Turbine System

Adam Rasheed,* Anthony H. Furman,† and Anthony J. Dean‡
General Electric Global Research,
Niskayuna, New York 12309

DOI: 10.2514/1.31893

A multitube pulse detonation combustor consisting of eight unvalved tubes arranged in a can-annular configuration was integrated with a single-stage axial turbine nominally rated for 10 lbm/s, 25,000 rpm, and 1000 hp. This pulse detonation combustor turbine system was operated using ethylene–air mixtures with each tube firing at 20 Hz. High-frequency pressure transducers were installed throughout the flow path to investigate the pressure-wave interactions and attenuation across the turbine. The multitube pulse detonation combustor was operated at a range of conditions with three firing patterns: a single tube firing, all tubes firing simultaneously, and all tubes firing sequentially. Analysis of these data reveal that wave interactions in the transition plenum between the pulse detonation combustor exit and turbine inlet plane can affect the optimum operation of the multitube pulse detonation combustor. In addition, a 20 dB attenuation of the peak pressure pulse and a 10 dB attenuation of the broadband acoustic noise through the single-stage, axial flow turbine were observed.

Nomenclature

dB_1	=	attenuation across turbine inlet to turbine exit
dB_2	=	attenuation across turbine inlet to exhaust duct
P	=	pressure
T	=	temperature
TTL_{db}	=	total transmission loss, dB

Subscripts

4	=	turbine inlet
5	=	turbine exit
6	=	exhaust duct

I. Introduction

PULSE detonation engines (PDEs) have been proposed for aerospace propulsion for more than 50 years [1] and have been considered for potential applications across the flight envelope spanning subsonic, supersonic, and hypersonic flight [2–4]. These engines rely on pressure-rise detonation, which is a supersonic shock-induced combustion wave [5], rather than constant-pressure deflagration currently used in aerospace propulsion engines. For a Chapman–Jouguet detonation, the incident shock wave and trailing combustion zone are coupled such that the temperature rise across the shock initiates the combustion whose subsequent heat release provides energy to sustain the shock. Many of the proposed propulsion applications rely directly on the impulse thrust of the detonation in a simple pure tube PDE configuration where the detonation exhausts directly into the ambient atmosphere. Advanced concepts have also been proposed such as hybrid-PDE gas turbine engine configurations where the standard steady flow deflagration combustor is replaced with multiple pulse detonation chambers (PDCs) as shown notionally in Fig. 1. PDEs have drawn attention because of their potential for increased specific impulse when compared to ramjets [6–9]. Furthermore, notional thermodynamic cycles show increased thermodynamic efficiency greater than Humphrey (constant volume) and Brayton (constant-pressure) cycles as a result of the pressure rise associated with a detonation [10–14].

Recently, there have been significant advances in the development of PDE technology with a focus on practical elements of single tube implementations. In particular, numerical and experimental investigations have focused on the importance of a converging–diverging exit nozzle to optimize the specific impulse [15–17], thrust augmentation using ejectors [18–20], detonation of liquid fuels [21–23], effect of ambient pressure [24], and nonintrusive laser-based time-resolved instrumentation [25,26]. The focus of this paper is to examine practical elements of a multitube PDC-turbine hybrid concept. Systems incorporating pressure-rise combustion upstream of a turbine were demonstrated as early as 1900 with the Holwitz explosion engine and more recent work with PDC-turbine hybrids is summarized in [27] by Rasheed et al. Although specific concepts vary in their implementation, a common feature incorporates the idea of the combustion products from the pulse detonation chambers driving a downstream turbine. Such configurations must address the challenges of the potential adverse impact of wave interactions on the operability of the PDCs, as well as understand the attenuation of the pressure waves as they pass through the turbine to assess the noise impact for commercial aviation applications.

It is thought that wave interactions in a multitube PDE system will affect its operability; however, these interactions have not been widely reported. Such wave interactions can either occur from firing of an adjacent PDE tube or from a reflection from downstream components, such as a common nozzle or a turbine. To date, there have been no quantitative investigations of a multitube PDE-turbine configuration, however, 2-D numerical simulations by Ebrahimi and Merkle [28] investigated multitube PDE geometries with a common converging–diverging exit nozzle. Their investigations examined dual-tube and three-tube configurations with and without splitter plates extending to the throat of the common nozzle in an attempt to isolate the PDE tubes from each other. In each simulation only a single tube was fired for one pulse. For the case without a splitter plate, their results showed the detonation wave diffracting at the PDE exit and propagating an upstream traveling shock wave in the adjacent tube with a pressure spike nearly as high as the original detonation pressure. It was conjectured that this shock wave would adversely affect the fill process of the adjacent tube, however, the

Presented as Paper 2006-1235 at the 44th AIAA Aerospace Sciences Meeting and Exhibit, Reno, NV, 9–12 January 2006; received 3 May 2007; accepted for publication 4 September 2008.

*Aerospace Research Engineer. Associate Member AIAA.
†Turbomachinery Research Engineer.
‡Manager, Propulsion Systems Laboratory. Member AIAA.

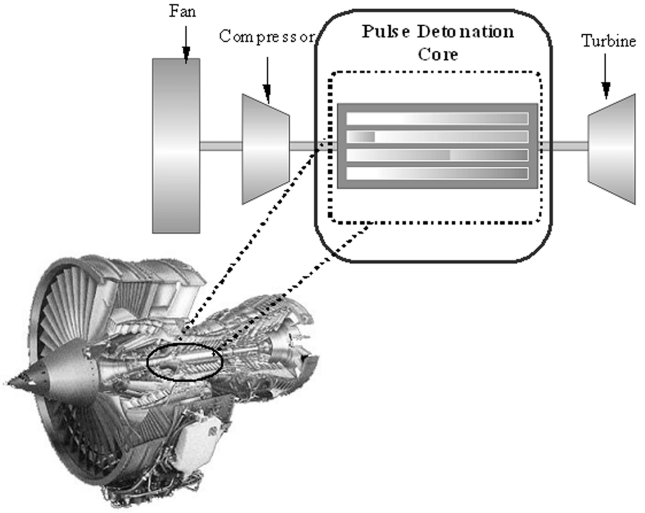

Fig. 1 PDC-turbine hybrid engine concept.

simulation of the detailed fill process was beyond the scope of this work. Conversely, it was found that the splitter plates were very effective and resulted in peak pressures in the adjacent tube as low as one-sixth the original detonation pressure depending on the details of the geometry.

More recent 2-D numerical investigations of a common-nozzle three-tube configuration performed by Ma et al. [29] added more insight because they modeled the full PDE cycle (fill, initiation, detonation, blowdown, purge) and included the effects of multicycle operation. The results showed upstream propagation of shock waves in adjacent tubes due to diffraction followed by a larger pressure pulse generated by a reflection from the internal wall of the common nozzle. For this study, the cycle frequency was extremely high (333 Hz per tube) such that the fill portion was complete before the pressure wave reached the head end. It was noted, however, that the pressure pulse would adversely affect the fill portion of the cycle for lower frequencies. Adding a splitter plate that extended from the PDE tube exit to the common-nozzle throat eliminated the dump plenum and showed an improvement in specific impulse. Analysis clearly demonstrated that wave interactions in the dump plenum were responsible for decreasing performance. These results were consistent from pulse to pulse once quasi-steady periodic operation was established after approximately five cycles.

Experimental data on wave interactions in multitube configurations are sparse and data on multitube systems firing into turbines are nonexistent. The first reported multitube device tested was a dual-tube PDE system with a common exit nozzle reported by Hinkey et al. [30]. The system was successfully operated at frequencies of up to 12 Hz per tube and was primarily used as a proof of concept that, in particular, tested the operability of a patented rotary valve inlet. No indication of the effect of wave interactions was provided. A subsequent follow-on five-tube PDE system was successfully tested with very little information publicly available. Photographs of the experimental setup, however, showed nozzles on each individual tube and perhaps wave interaction effects were less pronounced. Schauer et al. [31] has been successfully operating a 4-tube PDE system based on an automotive engine block. These tubes are far from each other and no wave interaction effects have been reported. Recently, Yatsufasu et al. [32] reported operation of a 4-tube PDE system firing into a common converging nozzle specifically designed to investigate wave interactions. Each of the tubes was instrumented with high-frequency pressure sensors, although no sensors were placed in the plenum at the PDE exit. The tubes were operated in a sequential firing pattern at 8 and 30 Hz (per tube) in a valved configuration using nominally stoichiometric H_2 air. The 30 Hz operating condition was found to propagate waves upstream into the adjacent tubes interfering with the deflagration-to-detonation transition (DDT) process. This resulted in delaying the arrival of the detonation wave and reducing the magnitude of the plateau pressure, which would decrease the thrust performance.

One of the main challenges with practical commercial implementations of a PDE-based propulsion device is the shock noise associated with the detonation wave exiting the engine. Simulations performed by He and Karagozian [33] predicted that the sound pressure level (SPL) of the detonation wave at the PDE tube exit could be as high as 200 dB. In addition, a variety of experiments have been recently performed with PDEs in anechoic chambers. Studies by Allgood et al. [34] measured far-field sound pressure levels of approximately 110 dB (along the tube centerline) with stoichiometric C_2H_4–O_2 mixtures at 100% fill in 25.4-mm (1 in.) diameter PDE tubes operating at less than 10 Hz. These studies highlighted the directivity of PDE acoustics and its sensitivity to engine operating conditions and exit nozzle geometry. Further studies by Glaser et al. [35] using the same PDE hardware showed that PDE-ejector configurations resulted in noise levels that were approximately 7 dB lower. Furthermore, the greatest noise reduction was in the lower frequencies associated with the shock noise, suggesting that components downstream of a PDE could greatly attenuate the magnitude of the peak pressure pulse.

Experimental acoustic measurements for PDC-turbine hybrid configurations are not as well reported in the open literature. Preliminary studies with a 2-D-PDE-cascade configuration used shadowgraph visualizations to observe the complex wave interactions as the detonation wave exited the PDE tube and interacted with the transition section and first row of turbine blades [36]. These experiments and computations qualitatively showed a strong reflection (and strong attenuation) of the incident wave across the cascade row. The first PDC-turbine experiments were performed on a small-scale rig by Schauer et al. [37] using a PDE coupled to the centrifugal turbine of an automotive-based turbocharger. It was qualitatively noted that high-frequency pressure transducers measured significant attenuation of the detonation wave through the turbine. The attenuation was quantified in recent preliminary studies, which tested a small-scale 6-tube PDC firing into a JFS-100-13A axial turbine and reported almost a 14 dB reduction in the pressure peak for a single tube firing into the turbine [38]. This rig consisted of an annular array of 25.4 mm (1 in.) tubes detonating stoichiometric C_2H_4–O_2 into a 6.1-in.-diam single-stage axial turbine with nominal rating of 1.6 lbm/s, 60,400 rpm, and 90 hp. The capability of a multitube PDC firing operation was still being developed with the anticipation of more noise and performance measurements. Further studies reported by Dean et al. [39] using a single tube impulse turbine (Elliott PYR partial admission steam turbine) rig with a rating of 1 lbm/s, 5000 rpm, and 100 hp also showed significant noise attenuation across the turbine, albeit the results were confounded because the PDE fired into a convoluted inlet with obstructions and safety valves between the PDE exit and turbine inlet. More significantly, the authors found only a 3 dB increase in sound power level during the PDE fired operation as compared to the baseline turbine spinning under steady flow.

Recent experiments tested a multitube PDC-turbine hybrid consisting of eight unvalved tubes arranged in a can-annular configuration integrated with a single-stage axial turbine nominally rated for 10 lbm/s, 25,000 rpm, and 1000 hp. The system accumulated 145 min of operation including many runs of 5+ min for the rig to achieve thermal steady state (as measured by the turbine stator metal temperature and the turbine inlet gas temperature) and for the turbine to attain constant speed. The rig was operated at frequencies up to 30 Hz (per tube) in different firing patterns using stoichiometric C_2H_4-air mixtures at conditions up to 8 lbm/s, 22,000 rpm, and 750 hp. A comprehensive dataset was obtained investigating operability, performance, and mechanical response [27]. This paper describes experiments investigating the detailed wave interactions at the turbine inlet plane and the wave attenuation across a single-stage axial turbine in a large-scale multitube PDC-turbine hybrid device representative of a potential aircraft propulsion system. The wave interactions throughout the rig, and, in particular, at the turbine inlet plane, were investigated with a focus on the effects of flow unsteadiness on overall operability. In addition, the

attenuation of the peak pressure pulse across the turbine was quantified for different operating conditions and firing patterns.

II. Experimental Setup

A. PDC-Turbine Hybrid System

For the present investigations, a PDC-turbine hybrid system was designed and built by integrating a multitube PDC system with a single-stage axial flow turbine. Figure 2 shows a solid model of the experimental rig. The multitube PDC consisted of eight unvalved PDCs arranged in a can-annular configuration on a 292 mm (11.5 in.) circle to line up as closely as possible with the midspan of the turbine blades [which was on a 305 mm (12 in.) circle]. The 6 mm (0.25 in.) offset between the tube centerline and the blade midspan was required for the tubes to fit into the standard 16-in. pressure vessel used for the outer case. The multitube PDC had an overall length of 1.5 m (5 ft). The downstream flange was designed to mate to either the turbine casing (turbocharger) or a standard 16-in. 300 lb flange so that the rig could also be tested by firing into a backpressured 16-in. pressure vessel rig (i.e., without turbomachinery downstream).

A cross section of the experimental apparatus is shown in Fig. 3. Each tube was 49.3 mm (1.939 in.) in diameter (2-in. schedule 80 pipe) with a length of 800.1 mm (31.5 in.) as measured from the downstream face of the fuel–air mixing element to the tube exit. This length was selected because it represented the distance in which C_2H_4-air detonation could be achieved using the implemented technology. A spark plug was mounted approximately one diameter downstream of the fuel–air mixing element to allow a short distance for the fuel and air to mix before ignition. A DDT geometry was used to assist the detonation process. Air was continuously flowed through the system (i.e., no valve on the air side), and the fuel injection was pulsed using two high-frequency valves mounted in parallel on each tube. Note that an orifice plate was used to choke the flow at the inlet to the primary plenum to isolate the facility piping from the rig. Each individual tube, however, was unchoked relative to the primary plenum. The effective area of each fuel valve had been independently determined experimentally and they were deliberately paired so that each PDC tube had the same net effective area across the fuel valves. High-speed shadowgraph imagery was used to verify that each of the valves had an open and close time of 2 and 5 ms, respectively. Each PDC was shrouded with a coaxial liner for secondary flow to provide backside cooling of the PDCs. This configuration for each PDC tube was chosen because of the extensive prior experience with similar configurations [22]. A rigorous risk reduction test program was conducted on a single tube implementation of the exact configuration before testing the multitube PDC.

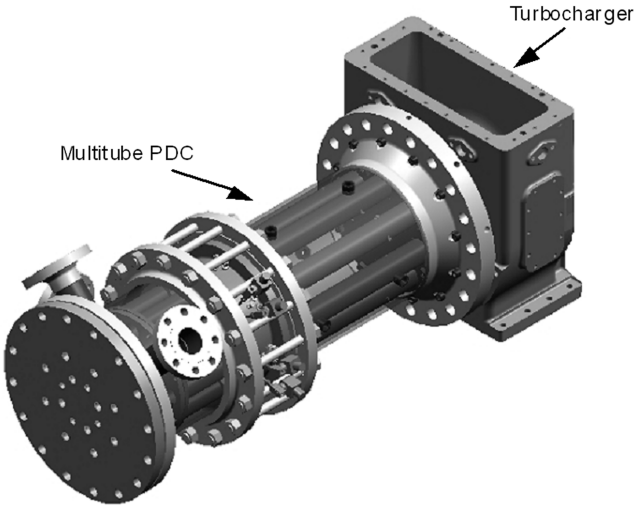

Fig. 2 Solid model of the PDC-turbine hybrid system used for the present experiments.

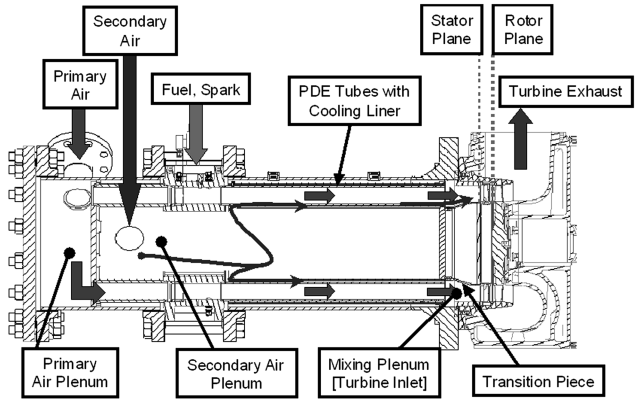

Fig. 3 Cross section of the PDC-turbine hybrid system.

The individual PDCs shared a common air inlet, as well as a common exit (in the transition region to allow for mixing) before entering the turbine. Furthermore, the secondary flow (bypass) air mixed with the primary detonated air in the transition region before entry into the turbine. Increasing the amount of cold secondary flow maintained the average temperature within the turbomachinery material temperature limits without changing the primary flow (and having to readjust the fuel fill and spark timing for the PDC). The transition piece consisted of a tapered truncated cone that matched the inner diameter (ID) from the PDE exit plane to the larger ID of the turbine inlet plane. The distance from the PDE exit to the stator inlet (i.e., the axial length of the transition piece) was 10.7 mm (4.2 in). The 356-mm (14 in) diameter single-stage axial turbine (1 stator and 1 rotor) was from a locomotive scale turbocharger designed for nominal flows of 10 lbm/s, 25,000 rpm, and 1000 hp. The compressor side of the turbocharger was on a separate air loop (drawing air from the ambient test cell) and used as the load for the turbine operation.

Throughout the design and manufacture, significant effort was made to ensure that each tube was geometrically identical and, whenever possible, an appropriate tuning knob was included in the design. This was deemed to be critical to minimize tube-to-tube variations during fired operations. For example, each PDC had an inlet flow adjustor that consisted of two slotted plates that could be rotated relative to one another to either decrease or increase the flow area to each tube. In this manner, each tube could be individually adjusted to have the same airflow rate. As described previously, the fuel valves were paired to match the effective areas to minimize any variation in fuel mass flow rate from tube to tube. In addition, the fuel valve manifold to the rig was specifically designed so that each tube had the same length of tubing from the common fuel manifold and each leg had a quarter-turn valve that could be used to adjust the fuel flow to each individual tube. The overall rig was designed for simplicity, ease of manufacturing and assembly, modularity for modifications, multiple access ports for instrumentation, and minimization of tube-to-tube variations.

B. Instrumentation

The PDC-turbine hybrid system was fully instrumented with mass flow measurements, flowpath temperatures and static pressures, surface thermocouples, an optical pyrometer, accelerometers, proximity probes for rotor dynamics, strain gauges, and an optical blade tip deflection measurement system. For the present investigation, the wave dynamics were captured using a number of high-frequency static pressure sensors (PCB 113A sensor) located throughout the rig. One sensor was located in the primary plenum, five were located in the turbine inlet plane (F plane) approximately 56 mm (2.2 in.) upstream of the stator leading edge, two were located in the turbine exit plane (Z plane) approximately 25 mm (1 in.) downstream of the rotor trailing edge, and one was located in the turbine exhaust duct as shown in Fig. 4. Note that PCB F0, F45, F90, and F225 were all directly in-line with a PDE tube, whereas F68 was

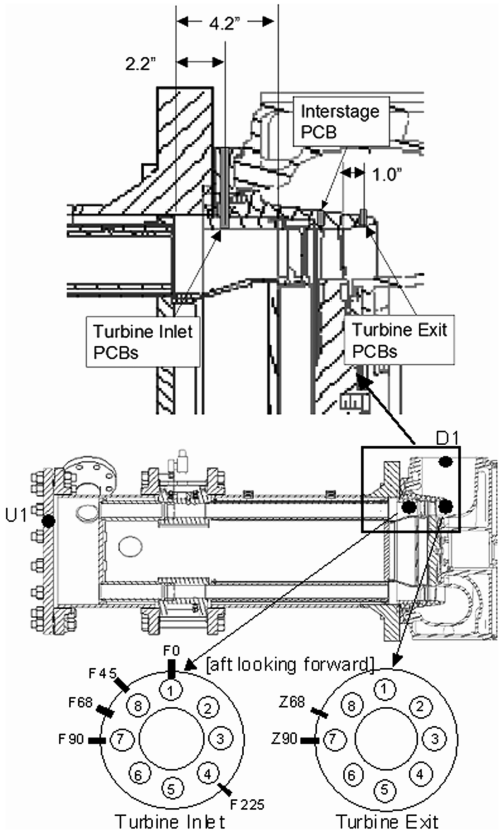

Fig. 4 Diagram showing locations of high-frequency piezoelectric pressure sensors (PCBs).

between tubes 7 and 8. Similarly at the turbine exit plane, PCB Z90 was geometrically in-line with tube 7, whereas PCB Z68 was between tubes 7 and 8. While the *Z*-plane transducers were immediately behind the rotor, PCB D1 was farther downstream in the exhaust duct after a significant area change and a 90 deg turn in the flow. All transducers were flush mounted with the local surface and were in direct contact with the flow. Pressure data were recorded at a 1 MHz sample rate using PC-based data acquisition systems based on National Instruments hardware. An additional high-frequency pressure sensor was added during the second test cell entry at the interstage location directly in-line with tube 7 (i.e., the 90 deg position). PCB N90 was approximately mid-distance between the trailing edge of the stator and the leading edge of the rotor. To measure detonation wave velocities, each tube was instrumented with two custom built, low-profile, high temperature ion probes located at 66 mm (26 in.) and 76 mm (30 in.) from the fuel–air mixer. The ion probe signals were measured at high frequency (1 MHz) in 1 s bursts, processed in real time to calculate the detonation wave velocities and the summary statistics were recorded at 1 Hz for the duration of the run. The ion probes verified that the Chapman–Jouguet (CJ) velocity of approximately 1850 m/s was achieved for each run condition.

C. Data Acquisition Systems

Four data acquisition systems were used to monitor the rig during its operation: a low-speed data acquisition system (DAQ) (∼1 Hz), a medium-speed DAQ (∼24 kHz), a high-speed DAQ (1 MHz), and the rotor shaft vibration monitoring DAQ. The low-speed DAQ consisted of two Yokagawa MX-100 with eight MX-110-UNV-M10 universal modules for a total of 80 channels. The data were monitored and collected using in-house data acquisition software. This was the primary means of monitoring the rig during operation and recording all flowpath temperatures and pressures, mass flow rates, and metal temperatures. The medium-speed DAQ consisted of a Teac LX-10 data recording system with a sample rate of either 24 or 48 kHz per channel. This system was used to record the strain gauge signals using Encore M610-002 strain gauge amplifier modules. The high-speed DAQ consisted of three separate desktop systems using National Instruments hardware. Each desktop had the capability of sampling eight channels at 1 MHz per channel and was configured with two PCI-6110 synchronized DAQ boards. They were connected to BNC-2011 patch panels using SH-68 cables. The high-speed DAQ was used to record the ion probe and PCB pressure transducer signals. The software was developed in-house with the particular feature of performing real-time processing of the ion probe signals into wave velocities that were then communicated and recorded on the low-speed DAQ. The rotor shaft vibration DAQ consisted of six capacitance probes to measure rotor displacement in the *X* and *Y* directions at the turbine bearing, compressor bearing, and compressor nose. The probes were monitored with a Bently Nevada ADRE system to provide rotor displacement and phase angle relationship in real time.

D. Control Systems

The PDC-turbine hybrid rig consisted of two independent control systems monitored by an operator. The Honeywell Test Cell Facility Control System was used to set the primary and secondary airflows and also provided the necessary turbine overspeed protections and automated emergency stop functions. The multitube PDC control system (MTPCS) developed in-house was used to set the timing for the spark and fuel valves for each PDC tube, the firing frequency, and the overall firing pattern. Once these parameters were set, the control system could be triggered to fire the multitube PDC for a desired duration. The MTPCS could operate the rig in excess of 40 Hz per tube, although for the present investigations, the firing frequency (per tube) was limited to 20 Hz. In addition to being able to fire any single tube individually, the MTPCS allowed the flexibility of firing the PDCs in any desired order. For the present experiments, the tubes were fired either simultaneously or sequentially.

III. Experimental Plan and Results

The PDC-turbine hybrid rig experiments were performed in two three-month test cell entries approximately six months apart. Typical rig operation consisted of establishing a desired prefire steady-state condition using the primary and secondary airflows (i.e., air flowing continuously through the rig without the PDCs firing). Once the turbine speed stabilized and it was determined that all pressures and temperatures were nominal, the multitube PDC was then fired for 1 s to obtain the gas dynamic wave interaction measurements. Two different firing patterns were tested: simultaneous and sequential. The simultaneous firing pattern consisted of firing all tubes at the same time at 20 Hz. The sequential pattern fired each tube individually at 20 Hz in sequence phased lagged by 0.125 s. Although not used for the present results, the rig had the capability to operate for a long duration (5 + min) to allow the turbine to spool up to its new PDC-fired steady-state condition for performance measurements. For those runs, the turbine would typically spool up to near constant speed within 30 s; however, performance measurements (i.e., work extraction) were only taken after 4 to 5 min when the rig reached thermal steady state. For the present work, the rig was operated for short durations (typically 1 to 5 s) during which the peak pressures and wave interactions throughout the rig were investigated using high-frequency pressure transducers. These tests durations were limited by the temperature specifications of the PCB sensors. Table 1 summarizes the run conditions tested in the present work.

The turbine speed was increased by maintaining the primary flow constant and increasing the secondary flow. The fill fraction was varied by changing the open and close timings for the fuel valve. The turbine pressure ratio was measured by a low-frequency (∼1 Hz) differential pressure transducer. Because the pressure downstream of the turbine was atmospheric, the turbine pressure ratio also represents the mean pressure (in atmospheres) in the PDC tube before firing. This mean pressure is important to note because it represents

Table 1 Experimental run conditions

Run	Frequency, Hz	Turbine pressure ratio	Turbine speed, rpm	Fill fraction
Condition A	20	1.18	7,700	0.91
Condition B	20	1.18	7,700	1.26
Condition C	20	1.16	7,450	1.38
Condition D	20	1.16	7,450	1.38
Condition E	20	1.40	11,500	1.19
Condition J	20	1.21	8,260	0.83

the baseline pressure in the PCB data shown in the subsequent sections. For each run condition, data were collected for each tube fired individually, all tubes fired simultaneously, and all tubes fired sequentially. Conditions A–E were obtained during the first test cell entry and condition J data were collected during the second test cell entry.

IV. Peak Pressure and Wave Interactions

A. Peak Pressure Measurements

Figure 5 shows the raw pressure trace from PCB F90 when tube 7 was fired at 20 Hz for 1 s using condition B. The right vertical axis shows the equivalent sound pressure level

$$\mathrm{SPL}_{\mathrm{dB}} = 10\log_{10}\frac{P_{\mathrm{peak}}^2}{P_{\mathrm{ref}}^2} = 20\log_{10}\frac{P_{\mathrm{peak}}}{P_{\mathrm{ref}}} \tag{1}$$

where P_{peak} is the peak pressure in absolute pressure units and P_{ref} is the "least audible sound" taken to be 2×10^{-5} Pa. In the plot, dots are used to mark the peak pressure for each pulse to help guide the eye. The average peak pressure for all 20 pulses was 305 ± 17 psi corresponding to a sound pressure level of 220 dB (shown as the dash-dotted line) which is consistent with the estimate by He and Karagozian [33]. The uncertainty was calculated as the standard error on the mean with a 95% confidence interval (i.e., if another 20 pulses were analyzed, there is a 95% probability that its mean would be within ± 17 psi). Note that the 2σ standard deviation for these peaks was much larger with a value of ± 37.9 psi (i.e., for the existing 20 pulses, 95% of the data lies within ± 37.9 psi). It should be noted that the peak pressure shown is the deviation from the mean pressure for this run condition (i.e., for condition B, the mean pressure was 17.2 psia, therefore the actual maximum pressure would be $305 + 17.2 = 322$ psia). The theoretical Chapman–Jouguet pressure (dashed line approximately 18 times initial pressure) is shown for reference on this plot. Most of the peaks are very close to this value, and the average is just slightly above. One explanation is that, although the detonation wave was weakening as it expanded out of the PDE tube into the unfueled transition plenum, the peak pressure remained high as a result of shock reflections on the transition piece geometry. In some cases, the peak pressure far exceeded the theoretical CJ pressure.

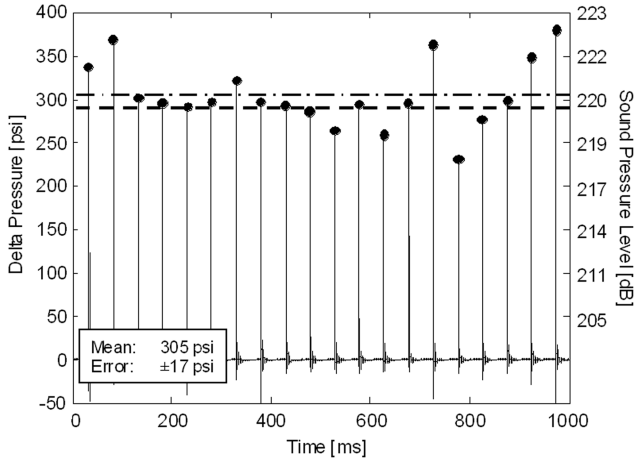

Fig. 5 Pressure time history for PCB F90 for firing of tube 7.

1. *Different Firing Patterns*

Figure 6a shows the raw pressure trace from PCB F90 when all the tubes were fired simultaneously at 20 Hz for 1 s using condition B. The average peak pressure measured was 287 ± 30 psi (dash-dotted line) which is just below the CJ pressure (dashed line) and within the uncertainty of the peak pressure measured for the case of a single tube firing. The larger variation in the peak pressures, however, suggests that wave interactions might be significant when firing all the tubes. Once again, the uncertainty was estimated as the standard error on the mean at 95% confidence. Figure 6b shows the raw pressure trace from PCB F90 when the tubes were fired sequentially at 20 Hz for 1 s using condition B. Within one firing cycle, there are multiple pressure peaks of lower magnitude corresponding to the waves generated from the other PDC tubes that were not directly in-line with PCB F90. Concentrating on the peaks generated by tube 7 (i.e., the tube directly in-line with PCB F90), the average was measured to be 201 ± 23 psi. The significantly lower mean value and large variation suggest that very severe wave interactions may be impeding the operability of the PDC tube. In fact, this particular time sequence shows several particularly low peak pressures around 200 and 700 ms indicating that the tube misfired.

The peak pressure data are summarized in Fig. 7, which shows a comparison of the peak pressures measured by PCB F90 (averaged over 20 pulses in a 1 s burst) for each of the run conditions and firing sequences. The peak pressures measured for the single tube firing

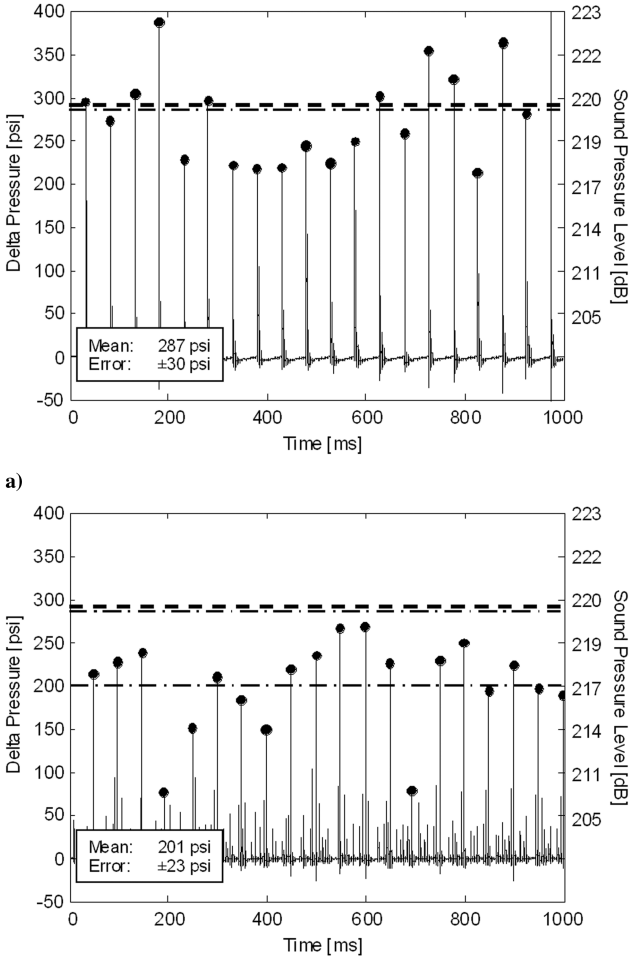

Fig. 6 Pressure time history of PCB F90 for a) simultaneous firing and b) sequential firing.

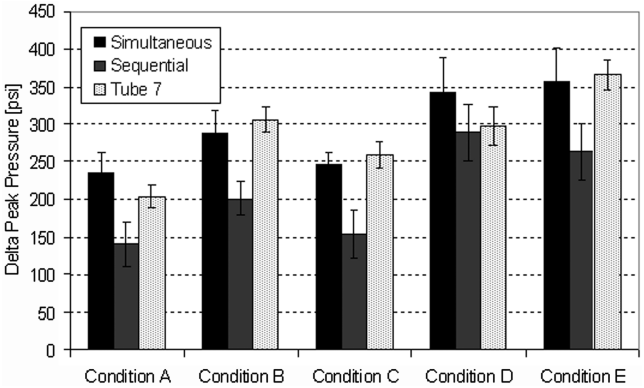

Fig. 7 Summary of the peak pressures for PCB F90 for each of the firing patterns.

(tube 7 only) and simultaneous firing are similar for most of the conditions (within the uncertainty), whereas the sequential pattern had a lower peak pressure for all run conditions. These observations were consistent across run conditions indicating that the trends were intrinsic to the firing pattern and not the result of the modifications to the fill fraction and fuel fill pressure.

As another measure of operability, Fig. 8 shows the percent variation (i.e., standard error divided by peak pressure) for the different firing patterns. This metric provides a measure of the pulse-to-pulse repeatability of the detonation peak pressures. It can be seen that, as expected, the single tube firing alone had the least variation (because there are no multitube interaction effects) and the sequential firing mode had the most variation.

2. *Upstream Propagation*

One important design feature of this particular rig was the valveless configuration on the upstream air inlet side to each pulse detonation chamber. As a result, the strong retonation wave was allowed to propagate freely into the upstream plenum with minimal obstruction. Although difficult to quantify, it was understood that this design choice would have an adverse impact on the performance as compared to a sealed head end. Less clear was the estimated magnitude of the upstream propagating pressure pulse and the impact it would have on the operability of the tubes. In a real engine implementation, such upstream propagating waves could adversely affect compressor performance, possibly leading to stall. Furthermore, the valveless configuration also likely allowed adverse tube-to-tube interactions at the head end, in addition to the tail of the PDCs. A PCB was placed in the upstream plenum to monitor the amplitudes of the upstream propagating waves. Figure 9 summarizes the peak pressures measured for the different firing patterns using all the conditions. As expected, the single tube firing resulted in the smallest pressure peak, and the simultaneous firing pattern resulted in the largest. The sequential pattern had the lowest upstream peak pressures and would be the most desirable by this measure.

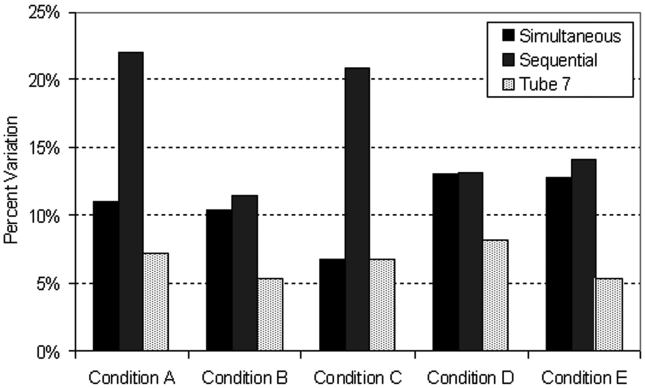

Fig. 8 Summary of percent variation in peak pressure for each of the firing patterns.

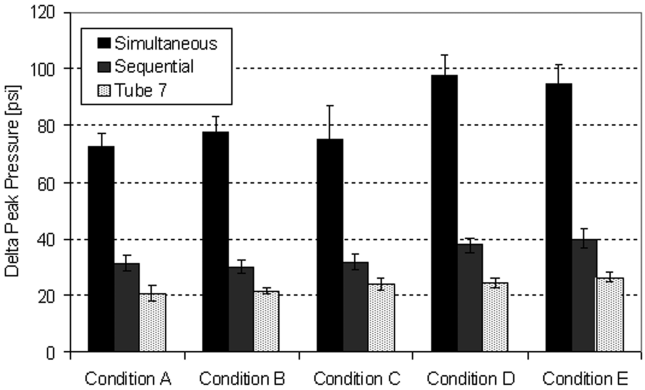

Fig. 9 Summary of peak pressure for PCB U1 for all the firing patterns.

B. Peak Pressures Through Rig

Figure 10a shows a summary of the peak pressures measured throughout the rig for the simultaneous firing pattern (averaged over 20 pulses) at condition B. The four pressure transducers at the turbine inlet plane directly in-line with the PDCs all measured approximately 300 psi. The two PCBs at the turbine exit measured approximately 30 psi and the PCB in the downstream duct showed negligible response because the wave was attenuated by the large area change into the exhaust duct. Details of the wave attenuation across the turbine are discussed in Sec. V. A similar plot for the sequential firing pattern is shown in Fig. 10b. The turbine inlet peak pressures are greatly reduced as compared to the simultaneous firing pattern, with PCB F0 and PCB F90 corresponding to tubes 1 and 7 having higher peaks than the other transducers. The sequential firing pattern caused all the tubes to operate poorly, with some much worse than others.

C. Pressure-Wave Interactions

Figure 11a shows the raw pressure traces for the second pulse from all the transducers in the turbine inlet (*F* plane) when tube 7 was fired

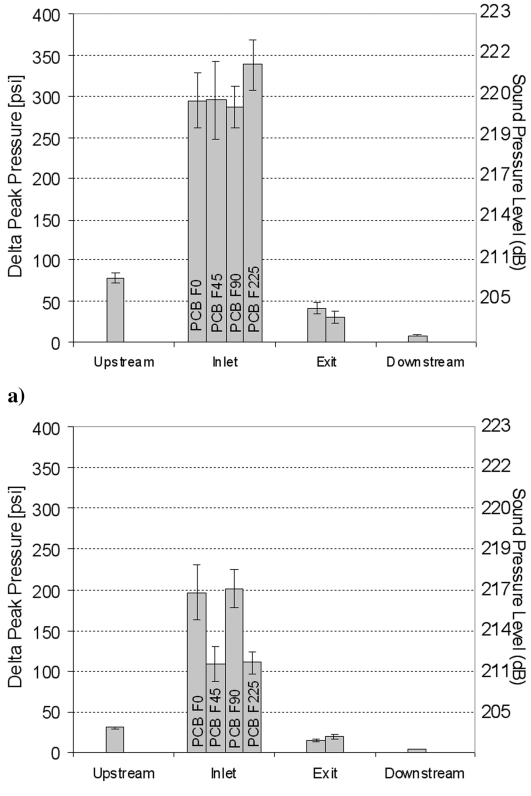

Fig. 10 Summary of peak pressures through the rig for a) simultaneous firing and b) sequential firing.

using condition B. The largest pressure peak of 300 psi was measured by PCB F90, which was directly in-line with tube 7 at the inlet plane. The arrival of the pressure wave is evident by the large pressure spike, followed by the very rapid decay in pressure as the wave weakens because it can relax around the annulus of the transition piece. The decaying wave travels around the annulus with PCB F225, which is almost 180 deg opposite, measuring the lowest peak of 30 psi and the largest delay in arrival time. Note that there is no evidence of a strong reflected wave from the stator because the wave is weakened as it diffracts and travels around the annulus and its impact is lost amidst the other wave interactions that are occurring. The pressure-time traces at each of the locations suggest very complicated wave interactions caused by the multifaceted 3-D geometry of the transition piece. The pressure-wave dynamics are completely attenuated within 6 ms of the arrival of the peak and the nominal steady flow is reestablished well before the arrival of the subsequent pressure wave.

Figure 11b showed similar traces when tube 5 was fired. The largest peak is measured to be approximately 100 psi, this time at PCB F225, which is closest to tube 5 (45 deg away). This amplitude is consistent with the data from Fig. 11a where PCB F45 (45 deg away from the fired tube 7) also had a peak amplitude of about 100 psi. The peak amplitude decreases as the wave travels around the annulus as seen in traces for PCB F90, PCB F68, and PCB F45. An increased peak of approximately 60 psi is seen in PCB F0, which is directly in-line with tube 1 (exactly 180 deg opposite tube 5 which was fired). This pressure rise is due to the constructive interference of the two waves generated by the firing of tube 5 traveling in opposite directions (clockwise and counterclockwise) around the annulus and colliding with each other in front of tube 1 (i.e., 180 deg around the annulus). These two cases of a single tube firing into a full annulus highlight the potential for complicated wave interactions that can occur in the full annulus transition piece and point toward adverse tube-to-tube interactions when multitube firing patterns are considered.

Recall that the simultaneous firing of all the tubes (Fig. 6a) showed large variation in the pressure peaks. It was hypothesized that this was due to wave interference from adjacent tubes. In theory, for the simultaneous firing case, the detonation waves should have all exited the PDC tubes at exactly the same time. Figure 12a, which shows the second pulse for all the transducers for the simultaneous firing at condition B, however, clearly demonstrates that the waves arrive at the PCB locations at slightly different times. PCBs F0, F45, F90, and F225 are all in-line with a PDC tube and show a scatter in the time of arrival of approximately 0.2 ms relative to one another. This is likely due to the slight difference in the DDT process in each of the tubes due to minor tube-to-tube geometric differences, and perhaps more significantly, flow differences due to turbulence effects. The effect of this scatter is to allow for the constructive and destructive interferences that would result in the large variation in peak pressure observed, likely resulting in a performance detriment.

The low peak pressures of the sequential firing of all the tubes (Fig. 6b) suggested that wave interactions were even more severe and adversely affected the operability of the adjacent tubes, perhaps by interfering with their purge and fill processes. Even more significant, it appeared that some tubes were intermittently disrupted completely and sometimes did not fire at all. It should also be noted that the sequential firing sequence sounded "roughest" when operating the rig. Figure 12b is an exploded view of the second firing cycle for all the pressure transducers for the sequential firing pattern at condition B. It clearly shows the multiple pressure peaks of lower magnitude corresponding to the waves generated from the other PDC tubes that were not directly in-line with PCB F90. Ideally, there should have been a total of seven minor pulses (corresponding to the other seven tubes); however, in this sequence tubes 8 and 4 did not fire (T1 is used to note the firing of tube 1, T2 for tube 2, etc.) during this cycle. This is not a systematic problem with these particular tubes because they do fire at other times within the same data set, while other tubes do not fire. For example, tube 8 fires at the very end of this time slice. A hypothesis is that the wave exiting one tube travels

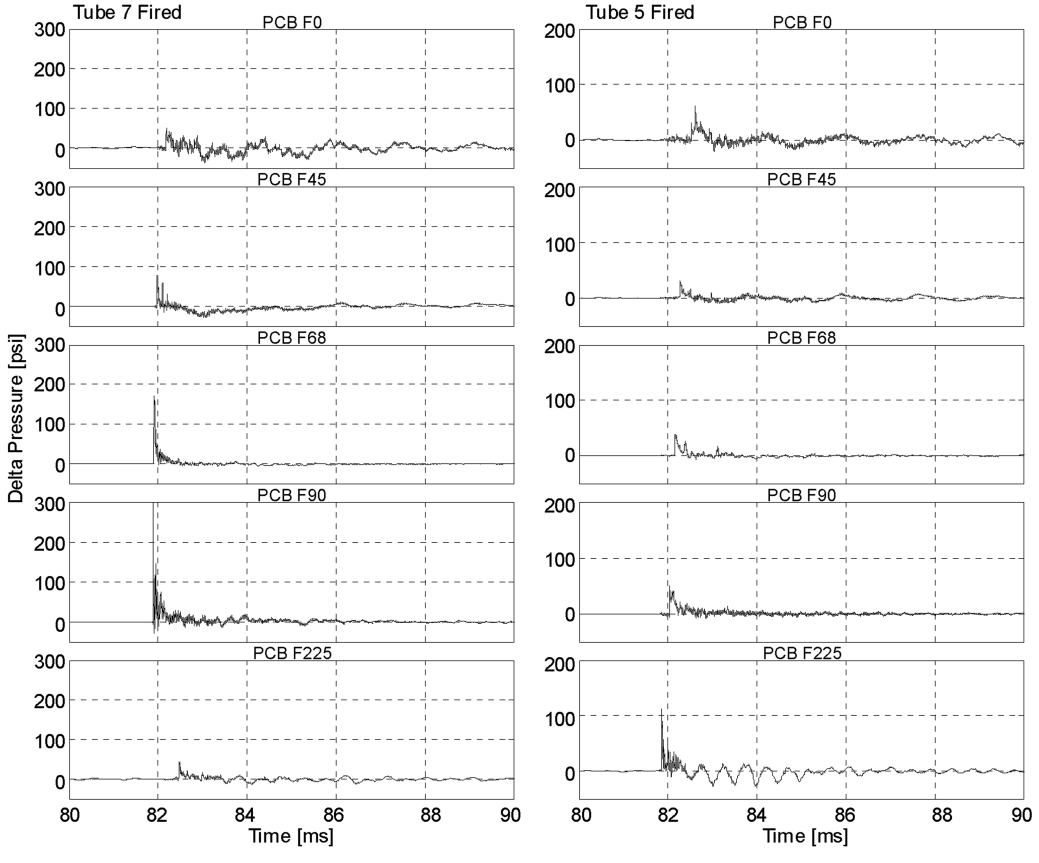

Fig. 11 Pressure time history for PCB F90 for second pulse using condition B when a) tube 7 is fired and b) when tube 5 is fired.

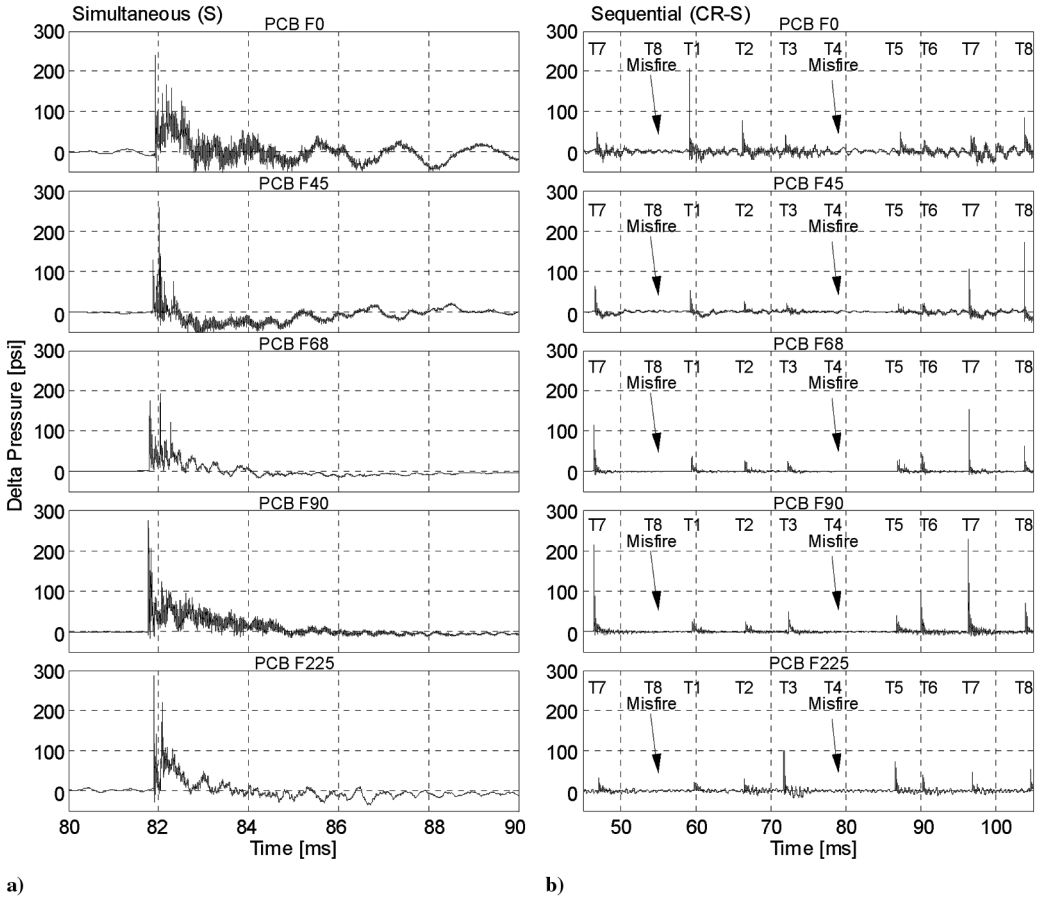

Fig. 12 Pressure time history for PCB F90 for second pulse using condition B for a) simultaneous firing and b) sequential firing.

upstream into an adjacent PDC, temporarily backpressuring the tube and perhaps even resulting in reverse flow. Because there were no pressure transducers on the PDC tube, it was not possible to verify this hypothesis or the strength of the wave. It is unclear whether this upstream propagating wave directly diffracted from the tube exit or whether it was a reflection off the transition piece or the stator. Regardless, it is apparent that the sequential firing pattern adversely affected the operability of the PDC tubes and is likely to result in suboptimal performance of the overall engine.

D. Effective Firing Frequency

To better understand the frequency content of the PDC acoustic signature, the power spectral densities (PSD) were calculated for selected runs using the full 1 s of data without any ensemble averaging. It was found that the pressure field responded with spectral peaks at the "effective firing frequency," defined as

$$f_{\text{eff}} = \frac{m f_{\text{tube}}}{n} \tag{2}$$

where m is the total number of PDCs, f_{tube} is firing frequency (per tube), and n is the number of tubes firing at one time. Figure 13a shows the PSD for PCB F90 for a simultaneous firing of all eight tubes at 20 Hz using condition B. The effective firing frequency for this simultaneous firing is 20 Hz ($m = n = 8$). The PSD shows spectral peaks at 20 Hz and its harmonics all the way up to 1 kHz, where there is a very sudden change in amplitude. Figure 13b shows the same plot for the sequential firing, where the overall amplitude of the signal is much lower than for the simultaneous case. The spectral peaks are at 160 Hz and its harmonic at 320 Hz. Although each tube was firing at 20 Hz, the flowfield responded at the effective firing frequency of all the tubes (i.e., eight tubes times 20 Hz). Very similar frequency responses were observed in PCB U1, which was in the upstream plenum, as well as PCB Z90, which was downstream of the turbine. It is clear that the entire flowfield throughout the rig was responding to the effective firing frequency. It should be noted that the PCB transducer vendor specifications indicated a resonant frequency greater than 500 kHz, so the present analysis is well within the operating limits of the sensor. This result is significant when understanding any potential acoustic coupling modes in the engine, as well as for understanding the mechanical forcing of components in a real engine application.

E. Summary of Wave Interactions for Different Firing Patterns

The results of the impact of wave interactions using both firing patterns are summarized in Table 2, which compares the two firing patterns in terms of the various metrics considered. The "higher" rating in the peak pressure category was given to the firing pattern that measured the highest peak pressure at the turbine inlet (i.e., PCB F90). For the spatial pattern factor, a better rating indicated a low standard deviation in the peak pressure measured from transducer to transducer. Similarly, a better rating for the temporal pattern factor was indicative of a low standard deviation in the peak pressures of subsequent pulses as measured by PCB F90. Finally, a "lower" rating in the upstream propagation category was indicative of a low peak pressure measured in the upstream plenum. It is important to note that this comparison is only valid for the present rig configuration. For example, valved configurations with downstream splitter plates could eliminate the operability issues with the sequential firing pattern. The more important point to note is that optimum multitube operation of a PDE will be a tradeoff between operability and performance.

V. Wave Attenuation Through the Turbine

One of the key discussions with regard to practical applications of PDEs concerns the noise signature as a result of the decaying blast wave traveling through and possibly exhausting out the back of the engine. Figure 14 tracks the pressure of the second pulse for tube 7

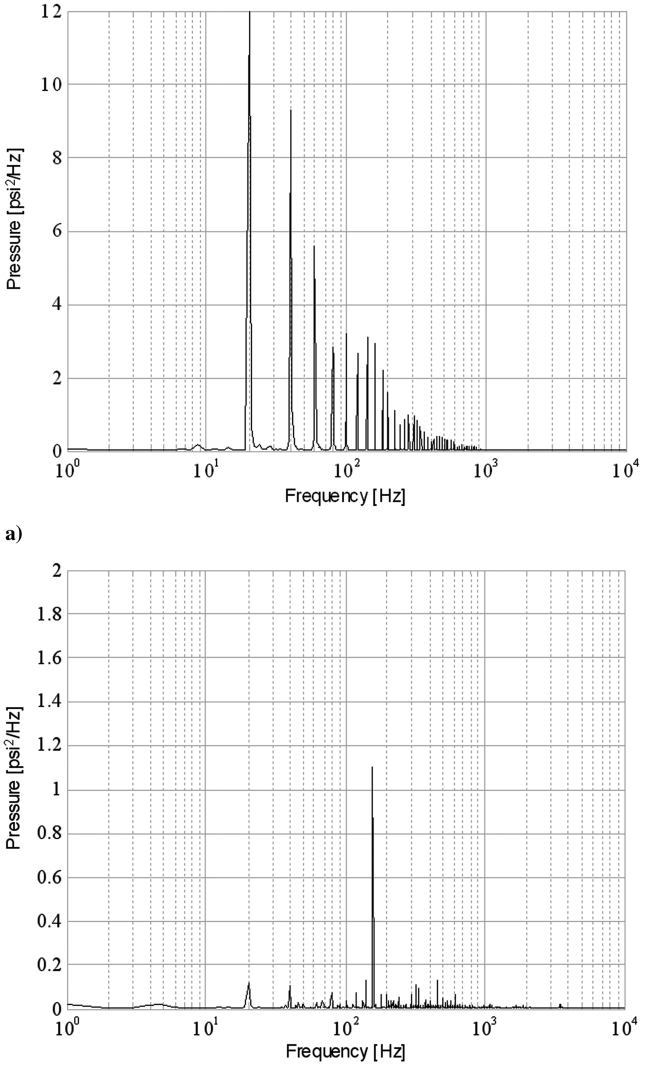

Fig. 13 PSD for PCB F90 (turbine inlet) for a) simultaneous firing and b) sequential firing.

fired using condition B as it travels through the turbine and into the exhaust duct. Figure 14a shows the pressure trace from PCB F90 with a peak pressure of about 300 psi. Figure 14b shows the pressure trace from PCB Z90 immediately downstream of the rotor and shows a significantly lower pressure of approximately 20 psi. This suggests that most of the energy of the peak pressure wave was reflected back upstream in the transition plenum and/or absorbed as mechanical vibration in the stator row. Figure 14c shows essentially no response measured by PCB D1 because the wave has been weakened significantly by the area change from the turbine exit plane to the exhaust duct.

This apparent attenuation of the detonation wave needs to be quantified and a method is described in Fig. 15. PDE noise can be characterized by three main phenomena: 1) the magnitude of the pressure peak (and its associated sound pressure level), 2) the attenuation of the pressure peak, and 3) the attenuation of the

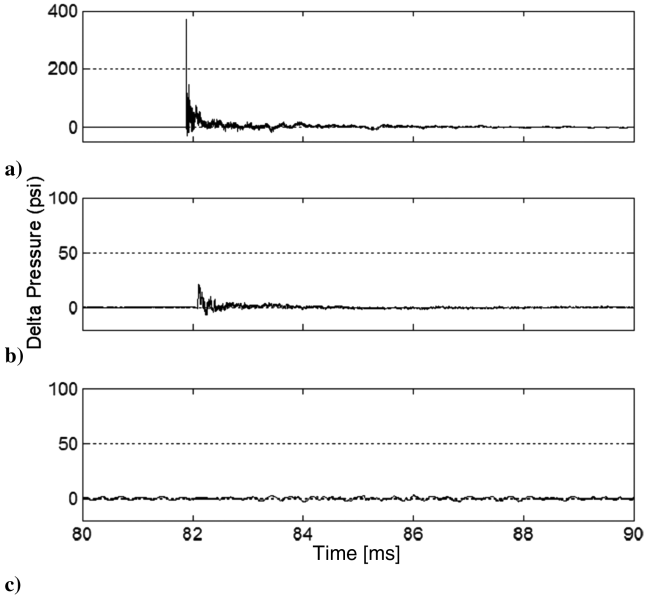

Fig. 14 Exploded views of the second pulse for tube 7 firing into the turbine for a) PCB F90, b) PCB Z90, and c) PCB D1.

broadband acoustic noise. The peak pressure magnitudes were discussed in detail in Sec. IV.A and were found to be approximately 220 dB at the PDC exit. The attenuation of the peak pressure and the broadband acoustic noise are discussed next.

A. Peak Pressure Attenuation

A key metric for the noise attenuation for a PDE is the peak pressure attenuation across the turbine, which can be calculated as

$$\mathrm{d\,B}_1 = 20\log_{10}\frac{P_4}{P_5} \qquad \mathrm{dB}_2 = 20\log_{10}\frac{P_4}{P_6} \tag{3}$$

where P_4 is the turbine inlet peak pressure measured using PCB F90, P_5 is the turbine exit peak pressure measured using PCB Z90, and P_6 is the peak pressure measured by the PCB D1 in the exhaust duct. With the above definitions, dB_1 is more closely related to the attenuation immediately across the single turbine stage, whereas dB_2 is the attenuation across the turbine stage and exhaust ducting.

Figure 16 shows the attenuation of the pressure peak (dB_1 and dB_2) measured across the turbine for different turbine speeds and compared with the most recent results reported by Caldwell et al. [38] for the case of a single tube firing (tube 7) into the turbine. It should be noted that the Caldwell results used a pressure transducer immediately downstream of the rotor and is comparable with our reported results for dB_1. The uncertainty on the present measurements is approximately ± 0.5 dB and is denoted by error bars. The present results for dB_1 show approximately 20 dB attenuation across the turbine stage. The lines are curve fits to help guide the eye and it can be seen that the present results suggest a slight increase in attenuation as turbine speed increases. More data are needed to confirm this trend as the present results are confounded because the fill fraction was also varied. The Caldwell results show approximately 28 dB reduction and virtually no trend with turbine speed. The difference in the magnitude of the attenuation is attributed

Table 2 Relative comparison of the operability of the different firing patterns

	Simultaneous	Sequential
Peak pressure	Higher peak P	
Qualitative sound	Smoother	
Pattern factor (spatial)	Lower standard deviation	
Pattern factor (temporal)		Lower standard deviation
Upstream propagation		Lower peak P

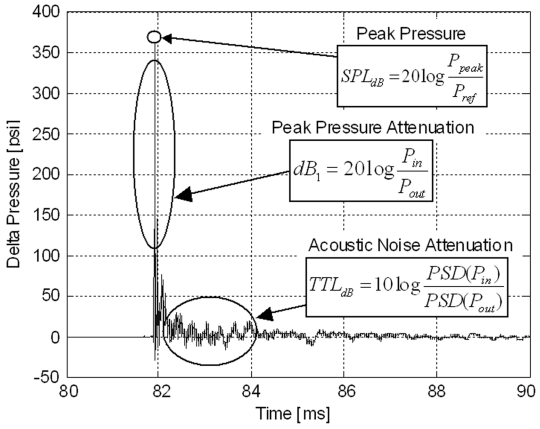

Fig. 15 Diagram showing the different contributions to PDE noise.

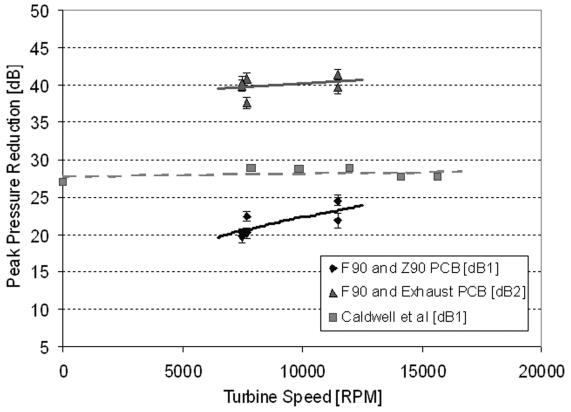

Fig. 16 Peak pressure reduction for a single tube firing into a turbine. The Caldwell et al. results are from [38].

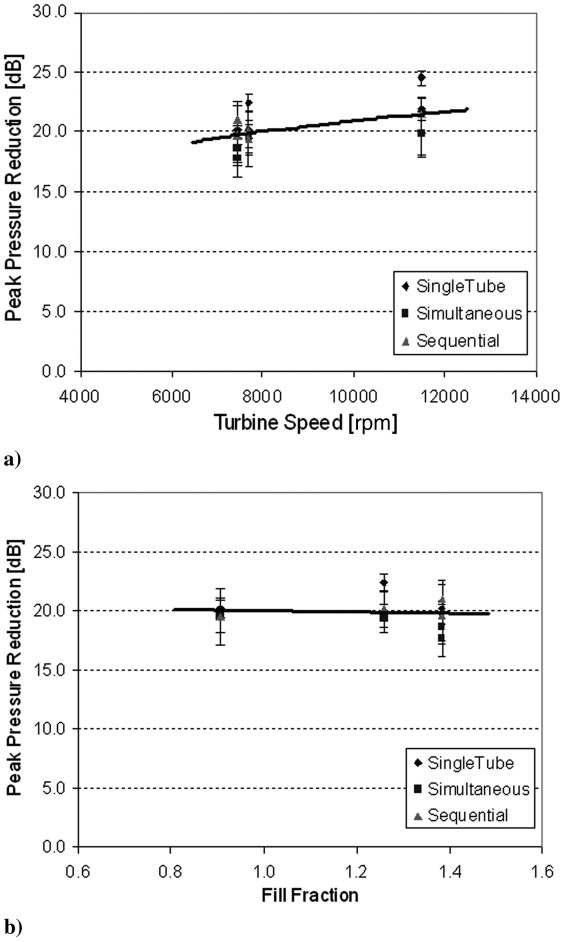

Fig. 17 Peak pressure attenuation dB1 as a function of a) turbine speed and b) fuel fill fraction.

to the very different geometries of the respective experiments. In particular, the turbine solidity (defined as the ratio of the blade spacing to the blade chord) for the present experiments was 1.5, whereas it was 2.0 for the Caldwell experiments. This 25% difference in solidity has the correct trend in that it results in a larger attenuation of the incident wave. The results for dB_2 show approximately 40 dB attenuation and virtually no trend with turbine speed. This suggests that the large area change into the exhaust plenum has a significant effect in damping the wave. The transition from the turbine exit plane to the exhaust plenum is highly geometry dependent, however, and it is more difficult to make comparisons with results from other experiments. For this reason, it is felt that the attenuation across the turbine stage (dB_1) is a more useful measurement and the remaining results are presented only for dB_1.

Figure 17a shows the effect of the firing pattern on the attenuation (dB_1) for the two firing patterns as a function of turbine speed with a curve fit to help guide the eye. As before, there is a trend suggesting an increasing attenuation as turbine speed increases; however, there is no obvious trend with the firing pattern. Despite the very different peak pressures measured for each of the firing patterns as described previously, the wave attenuation is approximately the same for all of them. This makes sense because wave attenuation expressed as the ratio of the magnitude of the transmitted over the incident wave is mostly a function of the area ratio of the constriction. Figure 17b shows similar data as a function of tube fill fraction where tube length does not include the distance of the transition region (i.e., distance between the PDE exit and the stator row). For this plot all the data were taken at roughly the same turbine speed and there is no trend observed with the fill fraction. Once again, there is no significant distinction between the attenuation for the different patterns. It should be noted that the fuel fill fraction is calculated based on the valve open time and the bulk flow velocity. The largest source of uncertainty was in the measurement for pressure used to estimate density in the calculation of the bulk fill velocity. The uncertainty in pressure was taken as the measured difference between the pressure at the inlet and exit of the PDE tube during the fill. Propagation of uncertainty analysis used to estimate the uncertainty in the fuel fill fraction is ± 0.1.

B. Broadband Noise Attenuation

The previous sections focused on the attenuation of the peak pressure of the shock wave. Although the majority of the noise emitted from the blast wave is an impulsive pressure rise, there may be significant contributions to the acoustic spectrum at other frequencies. For this reason, it becomes important to examine the attenuation across the entire frequency spectrum. The turbine transmission loss (TTL_{dB}) can be defined as

$$\mathrm{TTL}_{\mathrm{dB}} = 10\log_{10}\frac{\mathrm{PSD}(P_4)}{\mathrm{PSD}(P_5)} \tag{4}$$

where $\mathrm{PSD}(P_4)$ is the PSD of the turbine inlet pressure (PCB F90) and $\mathrm{PSD}(P_5)$ is the PSD of the turbine exit pressure (PCB Z90). Note that the constant in front of the log is 10 (not 20) because the PSD is effectively the square of the pressure. The PSDs used in this calculation were computed by dividing the 1 s time series into 10 groups (i.e., two pulses in each group because the rig was firing at 20 Hz), calculating the PSD for each of the groups, and then ensemble averaging over the groups. This was necessary to reduce numerical noise because we were dividing two highly processed signals.

Figure 18a shows the signal of TTL_{dB} for a single tube firing using condition B. Figures 18b and 18c show TTL_{dB} for the simultaneous and sequential fired cases, respectively. For the simultaneous case,

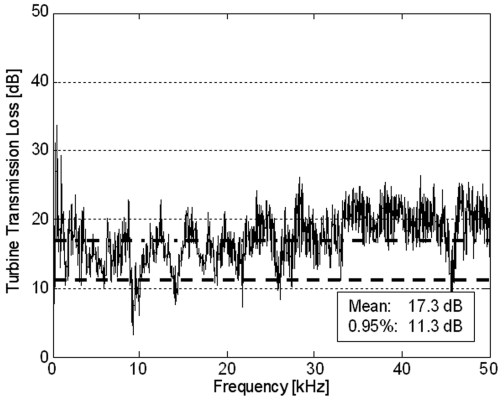

a)

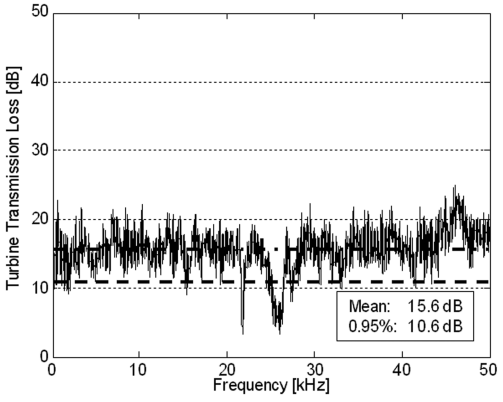

b)

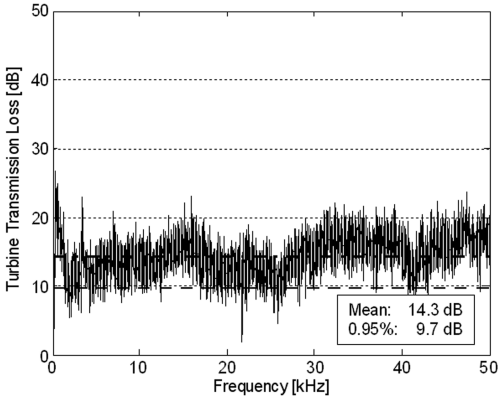

c)

Fig. 18 Broadband noise attenuation for a) tube 7 firing, b) simultaneous firing, and c) sequential firing using condition B.

the average attenuation across the spectrum is 17.8 dB, which is consistent with the peak pressure-wave attenuation of about 20 dB. It is clear, however, that there is less attenuation at certain frequencies. In particular, at 22 and 25 kHz there are narrowband regions where the attenuation is only 5 dB (or lower). Similarly for the sequential firing sequence, the average attenuation is 16.4 dB, with some frequencies less attenuated than others. Based on the frequency spectra, a conservative estimate for noise attenuation for the single-stage turbine would be 11 dB, as shown by the dashed line drawn on the plot, which represents the 95th percentile (i.e., 95% of the data lies above this line).

Figure 19 summarizes the TTL_{dB} for the single tube firing and both firing patterns using condition B. The mean across all the firing patterns is about 17 dB, and the 95% percentile is about 13 dB. As an additional check, the broadband noise attenuation was also characterized as the ratio of the root-mean-square (RMS) values of the turbine inlet pressure to turbine outlet pressure as calculated by

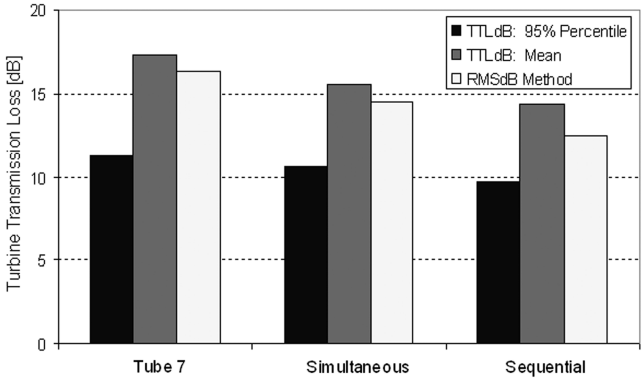

Fig. 19 Broadband noise attenuation for all firing patterns using condition B.

$$\mathrm{RMS}_{\mathrm{dB}} = 20 \log \frac{\mathrm{RMS}(P_4)}{\mathrm{RMS}(P_5)} \tag{5}$$

where $\mathrm{RMS}(P_4)$ is the root mean square of the turbine inlet pressure (PCB F90) and $\mathrm{RMS}(P_5)$ is the root mean square of the turbine exit pressure (PCB Z90). Figure 19 shows that the $\mathrm{RMS}_{\mathrm{dB}}$ value is close to the mean $\mathrm{TTL}_{\mathrm{dB}}$ for most of the firing patterns. A conservative estimate of a 10 dB reduction is a reasonable estimate for the noise attenuation across a single-stage turbine of this particular configuration.

C. Interturbine Stage Attenuation

To better understand the effect of the stator and the wave interactions experienced by the rotor, a study was performed by adding a PCB transducer at the interstage location (i.e., between the stator and rotor).

1. Peak Pressure Attenuation

Figure 20 tracks the details of the eighth pulse for the simultaneous firing pattern using condition J as it travels through the turbine. Figure 20a shows the pressure trace from PCB F90 with a peak pressure of about 200 psi. Figure 20b shows the interstage pressure trace from PCB N90, which is significantly attenuated (100 psi peak) and more importantly, exhibits a strong double peak behavior from the reflection of the wave between the stator and the rotor. The wave

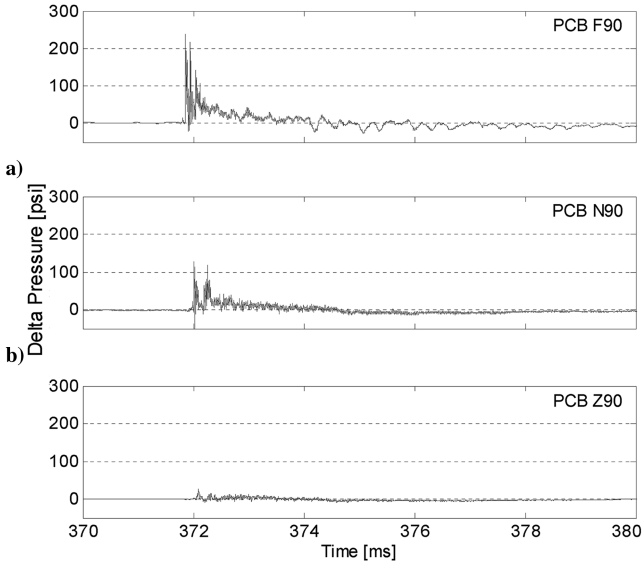

c)

Fig. 20 Exploded views of the eighth pulse for simultaneous firing into turbine for a) PCB F90, b) PCB N90, and c) PCB Z90 using condition J.

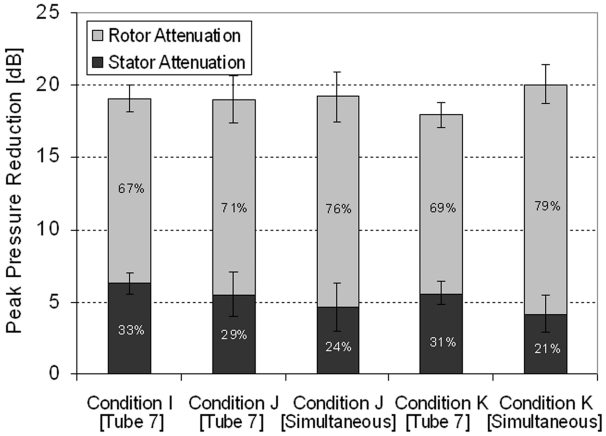

Fig. 21 Summary of peak pressure attenuation through the turbine.

is completely attenuated by 375 ms (i.e., within 3 ms of the initial peak), whereas PCB F90 is still showing response until 378 ms. Figure 20c shows the pressure trace from PCB Z90 immediately downstream of the rotor and shows significantly less response with a peak pressure of approximately 20 psi.

Figure 21 shows a summary of the peak pressure of the wave as it travels through the turbine for several different run conditions. The values were obtained by averaging the peaks measured over 20 pulses and the uncertainty bars shown represent the standard error on the mean with a 95% confidence interval. The total attenuation through the turbine is 19.1 dB (an average of the five runs considered in this chart), which is consistent with the data presented in Sec. IV.D. The relative contributions of the stator and rotor to the overall attenuation are highly dependent on the turbine details (e.g., bladed design, solidity, impulse or reaction turbine), however, for this particular turbine the majority of the attenuation occurred through the rotor. For the single tube firing cases, approximately 70% of the attenuation occurred in the rotor, whereas for the simultaneous firing cases, it was slightly higher at 80%. This is a somewhat counterintuitive result because it was expected that the stator would have been choked during the passage of the wave through the turbine, and as such would have been the larger contributor to the noise attenuation.

2. *Broadband Noise Attenuation*

The broadband noise attenuation through the turbine was also investigated. Figure 22 shows the PSD (computed as described in Sec. IV.D) for PCB F90, PCB N90, and PCB Z90 for simultaneous firing using condition J. The PSD for PCB F90 is very similar to the one discussed in Sec. IV.D. The amplitudes in PCB N90 are significantly lower with the highest peak response at 20 Hz, followed by its harmonics and a secondary peak at around 100 Hz. PCB Z90 had even lower amplitudes with the peak response at 100 Hz.

Figure 23 shows the turbine transmission loss, TTL_{dB} (calculated as described in Sec. V.B), through the individual components in the turbine. As before, the attenuation across the frequency spectrum shows localized minimums, with a mean attenuation of 12.4 dB across the turbine, which is consistent with the prior data. The stator is seen to attenuate the broadband noise by 3.2 dB and the rotor by 9.2 dB. The stator also shows negative attenuation (i.e., pressure rise) at certain frequencies (e.g., at 20 and 30 kHz), which could be the result of shock-on-shock interactions from wave reflections between the stator and the rotor. These experimental results compare well with numerical results obtained by Van Zante et al. for the attenuation of a detonation wave through a single stage axial turbine [40]. Van Zante et al. computed the "pressure transmission loss," which is identical to the TTL_{dB} of the present paper, to be approximately 4, 12, and 15 dB through the stator, rotor, and overall turbine, respectively. It should be noted that the two studies were done independently and the turbine configurations were different between the experimental and numerical investigations.

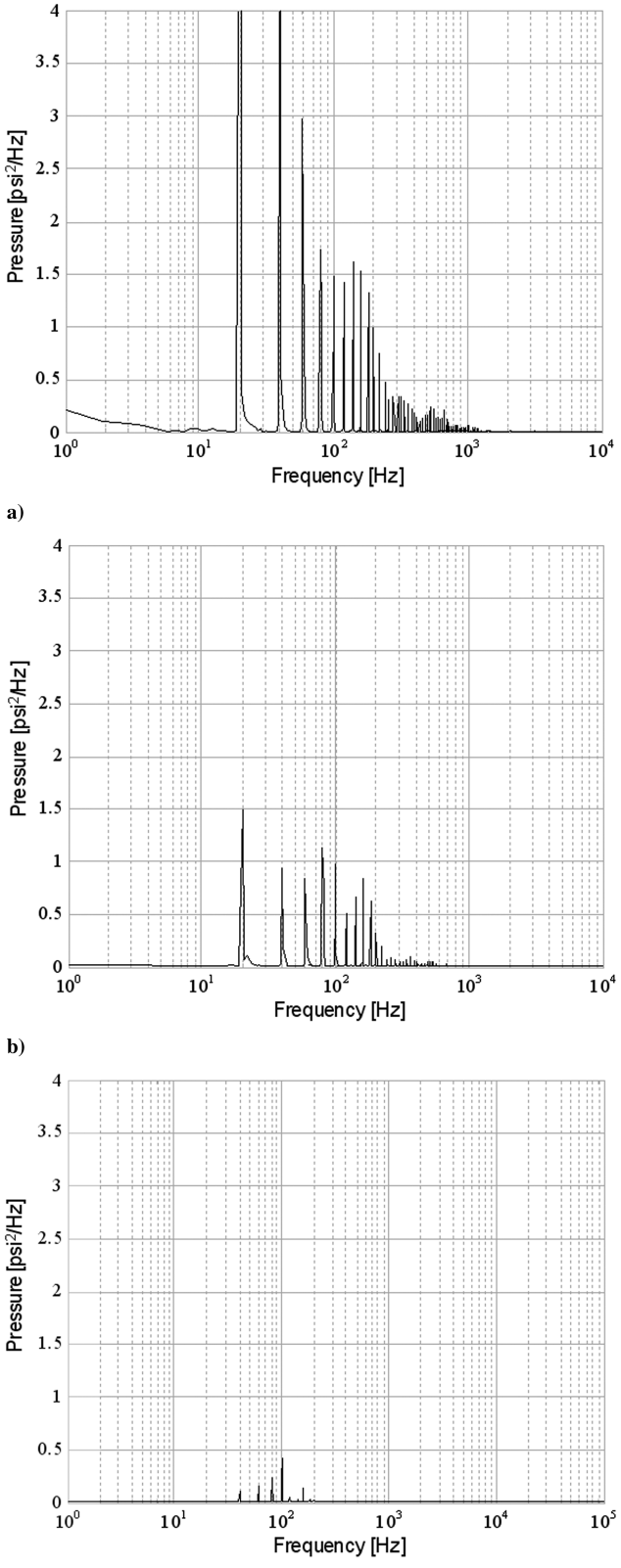

Fig. 22 PSD of a) PCB F90, b) PCB N90, and c) PCB Z90 for simultaneous firing using condition J.

Figure 24 summarizes the relative contribution of the stator and rotor to the broadband noise attenuation across the turbine for different run conditions. The total transmission attenuation was approximately 13 dB, which is consistent with the previously discussed data. As with the peak pressure, the broadband noise is also attenuated mostly by the rotor. The relative contribution of the rotor

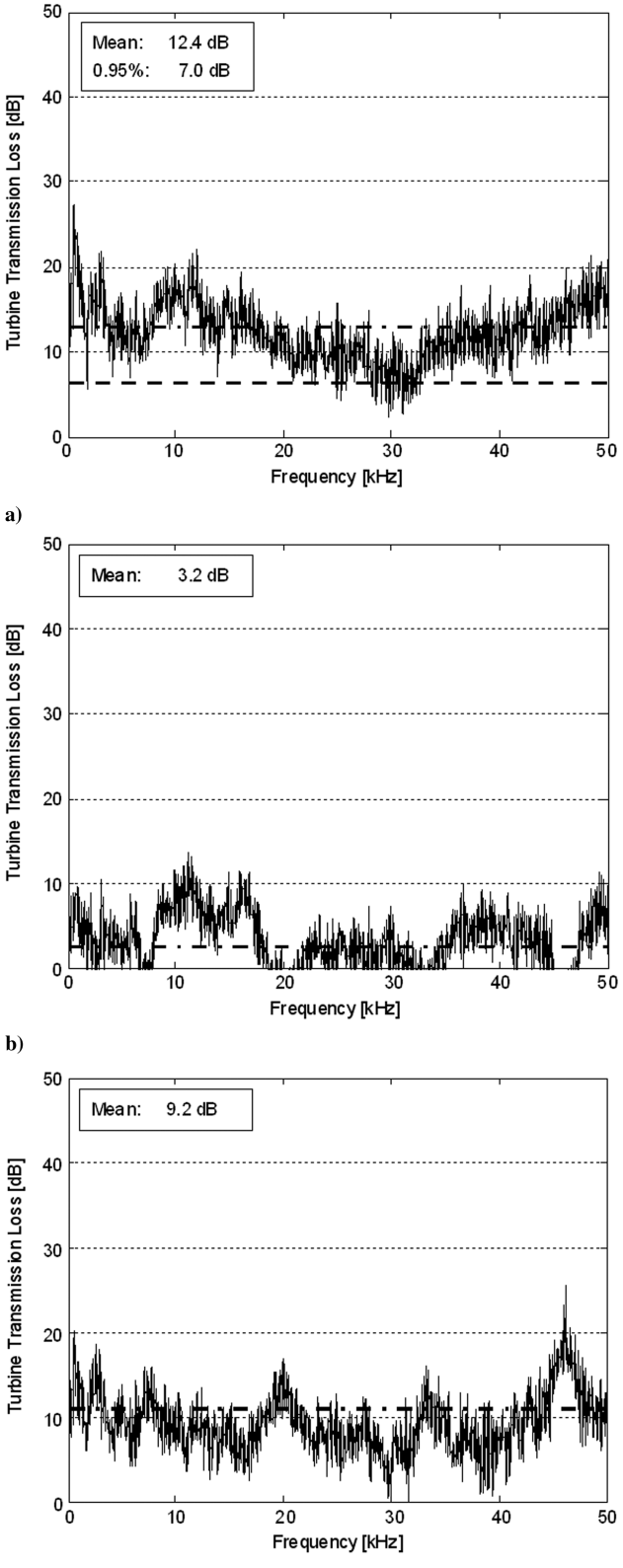

Fig. 23 Broadband noise attenuation across a) the turbine, b) the stator, and c) the rotor for simultaneous firing at condition J.

to the broadband noise attenuation is seen to be approximately 60% for the single tube firing and 75–80% for the simultaneous firing. For the single tube firing, the rotor has a smaller contribution to the attenuation of the broadband noise compared to the peak pressure. For the simultaneous firing, however, the rotor's contribution to both the peak pressure and broadband attenuation are the same.

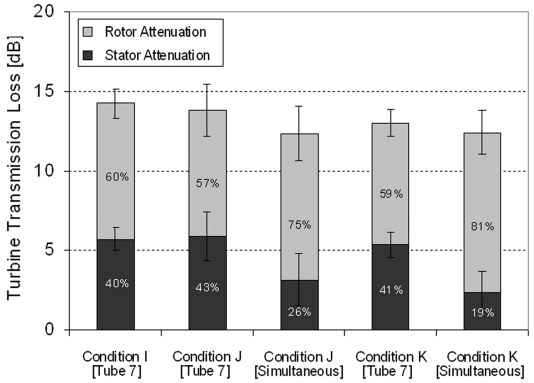

Fig. 24 Summary of broadband noise attenuation through the turbine.

VI. Conclusions

A multitube PDC with eight tubes arranged in a can-annular configuration integrated with a single-stage axial turbine nominally rated for 10 lbm/s, 25,000 rpm, and 1000 hp has been tested. High-frequency pressure transducers installed throughout the rig revealed complex wave interactions with significant downstream tube-to-tube interactions affecting operability when using the sequential firing pattern. Furthermore, the present valveless configuration allowed significant upstream propagation of pressure waves and backflow of detonation products with the possibility of upstream tube-to-tube interactions affecting operability. The 20 dB attenuation of the peak pressure pulse and 10 dB attenuation over the broadband acoustic spectrum across the single-stage turbine is promising and suggests that noise may not be a significant barrier to commercial applications of PDC-turbine hybrid engines. The results obtained from the present experiments represent only the beginning of the data required to understand the wave dynamics. Further PDC-turbine interaction studies are needed, in particular, at high pressure ratios more indicative of real engine operating conditions.

Acknowledgments

This work was performed as part of a collaborative effort between the General Electric Pulse Detonation Advanced Technology Program at the General Electric Global Research Center (GEGR) and the NASA Constant Volume Combustion Cycle Engine (CVCCE) program (Leo Burkardt, Program Manager) administered by the NASA Glenn Research Center. The authors recognize the technical input from Ed Envia (NASA Glenn Research Center), Clay Haubert, Venkat Tangirala, Mark Baptista, and Jonathan Janssen, as well as the technical support from Eric Cornell and Tony Brand. The hard work of Walt Chandler at GEGR is noteworthy for his role as the primary technician for all assembly, installation, and testing for the entire present experimental effort, as well for his technical expertise and experience.

References

[1] Nichols, J. A., Wilkinson, H. R., and Morrison, R. B., "Intermittent Detonation as a Thrust Producing Mechanism," *Jet Propulsion*, Vol. 27, No. 5, 1957, pp. 534–541.

[2] Roy, G. D., Frolov, S. M., Borisov, A. A., and Netzer, D. W., "Pulse Detonation Propulsion: Challenges, and Current Status," *Progress in Energy and Combustion Science*, Vol. 30, No. 6, 2004, p. 545. doi:10.1016/j.pecs.2004.05.001

[3] Kailasanath, K., "Recent Developments in Research on Pulse Detonation Engines," *AIAA Journal*, Vol. 41, No. 2, 2003, pp. 145–159. doi:10.2514/2.1933

[4] Powers, J., and Frolov, S. M., "Introduction Perspectives on Detonation-Based Propulsion," *Journal of Propulsion and Power*, Vol. 22, No. 6, 2006, pp. 1153–1154.

[5] Fickett, W., and Davis, W. C., *Detonation: Theory and Experiment*, Dover Publications, Mineola, NY, 2000.

[6] Wintenberger, E., Austin, J., Cooper, M., Jackson, S., and Shepherd, J., "Analytical Model for the Impulse of Single-Cycle Pulse Detonation

Tube," *Journal of Propulsion and Power*, Vol. 19, No. 1, 2003, pp. 22–38.
doi:10.2514/2.6099

[7] Wintenberger, E., and Shepherd, J., "Model for the Performance of Airbreathing Pulse-Detonation Engines," *Journal of Propulsion and Power*, Vol. 22, No. 3, 2006, pp. 593–602.
doi:10.2514/1.5792

[8] Ma, F., Choi, J.-Y., and Yang, V., "Propulsive Performance of Airbreathing Pulse Detonation Engines," *Journal of Propulsion and Power*, Vol. 22, No. 6, 2006, pp. 1188–1203.
doi:10.2514/1.21755

[9] Harris, P. G., Stowe, R. A., Ripley, R. C., and Guzik, S. M., "Pulse Detonation Engine as a Ramjet Replacement," *Journal of Propulsion and Power*, Vol. 22, No. 2, 2006, pp. 462–473.
doi:10.2514/1.15414

[10] Heiser, W. H., and Pratt, D. T., "Thermodynamic Cycle Analysis of Pulse Detonation Engines," *Journal of Propulsion and Power*, Vol. 18, No. 1, Jan.–Feb. 2002, pp. 68–76.
doi:10.2514/2.5899

[11] Kentfield, J. A. C., "Thermodynamics of Airbreathing Pulse-Detonation Engines," *Journal of Propulsion and Power*, Vol. 18, No. 6, 2002, pp. 1170–1175.
doi:10.2514/2.6075

[12] Goldmeer, J., Tangirala, V. E., and Dean, A. J., "System-Level Performance Estimation of a Pulse Detonation Based Hybrid Engine," *Journal of Engineering for Gas Turbines and Power*, Vol. 130, No. 1, Jan. 2008, p. 011201.
doi:10.1115/1.2771246

[13] Endo, T., "Thermodynamic Analysis of the Performance of a Pulse Detonation Turbine Engine," *Science and Technology of Energetic Materials*, Vol. 65, No. 4, 2004, pp. 103–110 (in Japanese).

[14] Deng, J., Chuanjun, Y., Zheng, L., Qiu, H., and Jiang, L., "Calculating Performance of Gas Turbine Engine with Embedded PDC," *Journal of Northwestern Polytechnical University*, Vol. 26, No. 3, June 2008, pp. 362–367 (in Chinese).

[15] Allgood, D. C., Gutmark, E., Hoke, J., Bradley, R., and Schauer, F., "Performance Measurements of Multicycle Pulse-Detonation-Engine Exhaust Nozzles," *Journal of Propulsion and Power*, Vol. 22, No. 1, 2006, pp. 70–79.
doi:10.2514/1.11499

[16] Owens, Z. C., and Hanson, R. K., "Single-Cycle Unsteady Nozzle Phenomena in Pulse Detonation Engines," *Journal of Propulsion and Power*, Vol. 23, No. 2, March–April 2007, pp. 325–337.
doi:10.2514/1.22415

[17] Cooper, M., and Shepherd, J. E., "Single-Cycle Impulse from Detonation Tubes with Nozzles," *Journal of Propulsion and Power*, Vol. 24, No. 1, 2008, pp. 81–87.
doi:10.2514/1.30192

[18] Wilson, J., Sgondea, A., Paxson, D., and Rosenthal, B., "Parametric Investigation of Thrust Augmentation by Ejectors on a Pulse Detonation Tube," *Journal of Propulsion and Power*, Vol. 23, No. 1, 2007, pp. 108–115.
doi:10.2514/1.19670

[19] Allgood, D. C., Gutmark, E., Rasheed, A., and Dean, A. J., "Experimental Investigation of a Pulse Detonation Engine with a Two-Dimensional Ejector," *AIAA Journal*, Vol. 43, No. 2, 2005, pp. 390–398.
doi:10.2514/1.8125

[20] Glaser, A. J., Caldwell, N., Gutmark, E., Hoke, J., Bradley, R., and Schauer, F., "A Study on the Operation of Pulse Detonation Engine Driven Ejectors," *Journal of Propulsion and Power* (to be published).

[21] Kailasnath, K., "Liquid-Fueled Detonations in Tubes," *Journal of Propulsion and Power*, Vol. 22, No. 6, 2006, pp. 1261–1268.
doi:10.2514/1.19624

[22] Frolov, S. M., "Liquid-Fueled, Air-Breathing Pulse Detonation Engine Demonstrator: Operation Principles and Performance," *Journal of Propulsion and Power*, Vol. 22, No. 6, 2006, pp. 1162–1169.
doi:10.2514/1.17968

[23] Jian-Zhong, L., "Investigation on Common Nozzle of Triple-Tube Pulse Detonation Engine with Kerosene/Air," *Journal of Aerospace Power*, Vol. 23, No. 5, May 2008, pp. 840–844 (in Chinese).

[24] Cooper, M., and Shepherd, J. E., "Detonation Tube Impulse in Subatmospheric Environments," *Journal of Propulsion and Power*, Vol. 22, No. 4, 2006, pp. 845–851.
doi:10.2514/1.16979

[25] Mattison, D. W., Brophy, C. M., Sanders, S. T., Ma, L., Hinckley, K. M., Jeffries, J. B., and Hanson, R. K., "Pulse Detonation Engine Characterization and Control Using Tunable Diode-Laser Sensors," *Journal of Propulsion and Power*, Vol. 19, No. 4, 2003, pp. 568–572.
doi:10.2514/2.6167

[26] Klingbeil, A. E., Jeffries, J. B., and Hanson, R. K., "Design of a Fiber-Coupled Mid-Infrared Fuel Sensor for Pulse Detonation Engines," *AIAA Journal*, Vol. 45, No. 4, 2007, pp. 772–778.
doi:10.2514/1.26504

[27] Rasheed, A., Furman, A. H., and Dean, A. J., "Experimental Investigations of an Axial Turbine Driven by a Multi-Tube Pulsed Detonation Combustor System," AIAA Paper 2005-4209, 10–13 July 2005.

[28] Ebrahimi, H. B., and Merkle, C. L., "Wave Reverberations in a Multitube Pulse Detonation Engines," *Journal of Propulsion and Power*, Vol. 24, No. 2, March–April 2008, pp. 345–352.
doi:10.2514/1.32162

[29] Ma, F., Choi, J-Y., and Yang, V., "Thrust Chamber Dynamics and Propulsive Performance of Multitube Pulse Detonation Engines," *Journal of Propulsion and Power*, Vol. 21, No. 4, July–Aug. 2005, pp. 681–691.
doi:10.2514/1.8182

[30] Hinkey, J. B., Williams, J. T., Henderson, S. E., and Bussing, T. R. A., "Rotary-Valved, Multiple-Cycle, Pulse Detonation Engine Experimental Demonstration," AIAA Paper 1997-2746, 6–9 July 1997.

[31] Schauer, F., Stutrud, J., Bradley, R., Katta, V., and Hoke, J., "Detonation Studies and Performance Results for a Research Pulse Deetonation Engine," *Confined Detonations and Pulse Detonation Engines*, edited by G. Roy, S. Frolov, R. Santoro, and S. Tsyganov, Torus Press, Moscow, Russia, 2003, pp. 275–290.

[32] Yatsufusa, T., Nishimura, K., Yamaguchi, T., and Yoshinaga, K., "Experiments on Inter-Tube Interference in a Four-Tube Pulse Detonation Engine," *Proceedings of the 20th ICDERS*, McGill University, Montreal, Canada [CD-ROM], 31 July –5 Aug. 2005.

[33] He, X., and Karagozian, A., "Pulse-Detonation-Engine Simulations with Alternative Geometries and Reaction Kinetics," *Journal of Propulsion and Power*, Vol. 22, No. 4, July–Aug. 2006, pp. 852–861.
doi:10.2514/1.17847

[34] Allgood, D., Glaser, A., Caldwell, N., and Gutmark, E., "Acoustic Measurements of a Pulsed Detonation Engine," AIAA Paper 2004-2879, 10–12 May 2004.

[35] Glaser, A., Caldwell, N., and Gutmark, E., "Experimental Investigation into the Acoustic Performance of a Pulse Detonation Engine with Ejector," AIAA Paper 2005-1345, 10–13 Jan. 2005.

[36] Rasheed, A., Tangirala, V. E., Vandervort, C. L., and Dean, A. J., "Interactions of a Pulsed Detonation Engine with a 2D Turbine Blade Cascade," AIAA Paper 2004-1207, 5–8 Jan. 2004.

[37] Schauer, F., Bradley, R., and Hoke, J., "Interaction of Pulsed Detonation Engine with a Turbine," AIAA Paper 2003-0891, 6–9 Jan. 2003.

[38] Caldwell, N., Glaser, A., and Gutmark, E., "Acoustic Interactions of a Pulse Detonation Engine Array with a Gas Turbine," AIAA Paper 2006-1233, 9–12 Jan. 2006.

[39] Dean, A. J., Rasheed, A., Tangirala, V. E., and Pinard, P. F., "Operation and Noise Transmission of an Axial Turbine Driven by a Pulse Detonation Combustor," *Proceedings of the International Gas Turbine Institute*, GT-2005-69141, American Society of Mechanical Engineers, Fairfield, NJ, 6–9 June 2005.

[40] Van Zante, D., Envia, E., and Turner, M., "The Attenuation of a Detonation Wave by an Aircraft Engine Axial Turbine Stage,"NASA TM-2007-214972; also ISABE Paper 2007-1260 at the 18th ISABE Conference, Beijing, China, 2007.

J. Powers
Associate Editor